Unidirectional coupling of a quantum emitter to a subwavelength grating waveguide with an engineered stationary inflection point

Ilya A. Volkov and Roman S. Savelev*
School of Physics and Engineering, ITMO University, Saint Petersburg 197101, Russia

(Received 8 September 2021; accepted 11 November 2021; published 8 December 2021)

In this work, we propose an approach for the design of a waveguide structure that allows for efficient and highly asymmetric coupling of the quantum sources with circularly polarized transition dipole moments to the guided mode of the structure. The approach is based on the mixing of the two quasidegenerate modes of a periodic waveguide with an auxiliary single-mode waveguide leading to the formation of the dispersion with a stationary inflection point and consequently to the high coupling efficiency of this mode with a dipole source. We show that the distribution of the field polarization inside the waveguide is relatively homogeneous, maintaining the circular polarization in a large area. Consequently, this leads to a high degree of tolerance of the coupling asymmetry and strength to the position of the quantum emitter. We believe that our results will extend the variety of designs of the efficient chiral nanophotonic interfaces based on planar semiconductor nanostructures.

DOI: 10.1103/PhysRevB.104.245408

I. INTRODUCTION

Tailoring of the light-matter interaction at nanoscale has attracted a lot of attention in the last decades due to increased technological capabilites of creating various optical nanostructures and their potential in the development of compact and scalable quantum-integrated components based on the deterministic nanophotonic interfaces between the quantum emitters (QE) and light. One of the recently proposed ways to achieve this goal is based on the so-called chiral light-matter interaction [1], which manifests itself in an asymmetric interaction between the QEs with circularly polarized dipole transition moments and localized optical modes propagating in opposite directions.

All studies that utilize effects based on the chiral light-matter interaction can be categorized based either on the type of the QEs or on the type of the photonic nanostructures employed in the design. From the "matter" point of view one can distinguish a few main platforms including cold atoms [2–4], semiconductor quantum dots [5], and two-dimensional materials [6]. Each of them, however, possesses specific features and limitations related to their experimental realization. Therefore, quite a variety of photonic nanostructures were theoretically and experimentally investigated in application to these platforms, including photonic crystal waveguides [7,8], homogeneous optical nanowaveguides [9–13], whispering gallery-type resonators [2,14,15], and, more recently, topological semiconductor waveguides and resonators [16–19]. Arguably one of the most suitable technologies for the practical purposes is based on a semiconductor GaAs platform that allows for integration of planar optical waveguides and cavities with quantum dots and efficient control of their emission properties [5,20,21]. Several studies have experimentally demonstrated asymmetry of coupling of a quantum dot to a waveguide close to 100% [8,10,13,22,23]. In addition, the strength of the coupling can also be increased when employing a cavity or slow-light modes of photonic crystal (PhC) waveguides or cavities [8,16–18,22]. However, both coupling asymmetry and strength in such systems remain sensitive to the position of the QE due to the rather inhomogeneous field distribution in the unit cell of the PhC.

Lately, an alternative to the PhC-based systems in the form of various nanostructures composed of Mie resonant dielectric and semiconductor nanoparticles has been extensively explored [24,25]. Such a bottom-up approach allows one to design structures with different geometry and with different optical properties by careful tuning of their individual building blocks and coupling between them. This includes single nanoantennas and their ensembles for control of the QE luminescence radiation patterns [26–30], optical cavities and waveguides composed of dielectric and semiconductor nanoparticles for the Purcell enhancement and lasing [31–34], and active metasurfaces [35,36]. In this context, periodic dielectric waveguides provide vast opportunities for dispersion engineering [37–39] and achieving slow light regimes for efficient modulation of optical signals [40] as well as polarization control due to the mode degeneracy engineering [41–43].

In this work, we propose an approach for the design of an optical nanostructure based on a periodic waveguide that can serve as an efficient chiral interface between the propagating waveguide modes and the circularly polarized dipole sources embedded in the structure. This approach relies on two factors: the presence of two quasidegenerate orthogonal modes in a periodic waveguide, and a specific type of the dispersion of the whole structure possessing a stationary inflection point (SIP). The combination of these factors leads to the increase the strength of the light-matter interaction while at the same time maintaining its high level of asymmetry. Moreover, unlike other designs studied before, the coupling of a quantum

*r.savelev@metalab.ifmo.ru

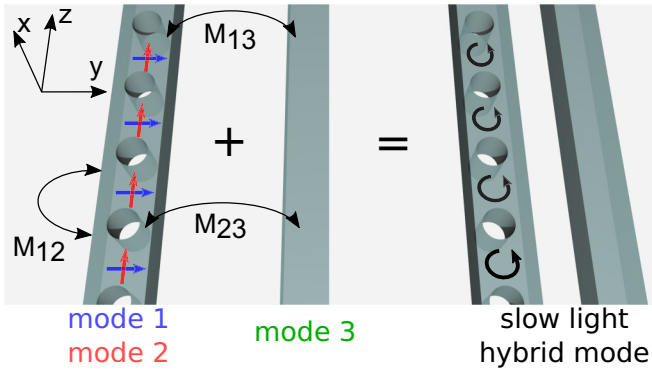

FIG. 1. Scheme of the considered system: two orthogonal modes of a periodic waveguide and a single mode of a homogeneous waveguide couple with each other forming a single supermode with low group velocity and local circular polarization of the field inside the periodic waveguide. Arrows indicate the dominant polarization of the field.

source to the mode of the proposed structure is substantially more tolerant to the position of the source, which makes it beneficial from the practical point of view. We believe that the presented results will allow for the development of the advantageous bottom-up designs of compact chiral nanophotonics interfaces for efficient and scalable integrated quantum circuitry.

II. FORMULATION OF THE IDEA

The design of the proposed waveguiding structure that allows for efficient and uniform coupling with circularly polarized dipole emitters is based on a specific type of the waveguide dispersion $\omega(k)$ that contains a stationary inflection point, i.e., a point at which the group velocity $d\omega/dk$ and the group velocity dispersion $d^2\omega/dk^2$ vanish. It is known that such type of dispersion emerges when at least three modes are coupled in a specific way, forming an exceptional point of degeneracy of the third order [44–46]. In the current work we consider a structure in which two of the three modes belong to the same periodic waveguide and the third one belongs to the auxiliary spatially separated homogeneous waveguide, as schematically shown in Fig. 1. If two quasidegenerate modes of the periodic waveguide have local electric field polarization orthogonal to each other, then the polarization of the mixed mode of the coupled waveguides will be elliptical in general, with the specific type of polarization depending on the type of the coupling between the modes. Further, if the characteristics of the third mode are chosen in a proper way, the mixed mode will possess a SIP in the dispersion.

Such a mode of the structure exhibits several features beneficial for the chiral light-matter interaction. First, the group velocity of the mode tends to zero at a certain frequency, providing a potential for an arbitrarily strong coupling of the point dipole source to the guided structure. Second, by tuning the geometrical parameters of the structure, one can effectively control a type of the coupling between the modes, which determines the local field polarization of the mode. Thereby, one can design a waveguide with circular local polarization of the electric field and thus reach the fully asymmetric coupling of the dipole source to the modes propagating in forward and backward directions along the waveguide. Finally, the distributions of the field of uncoupled modes, which can be considered as rather homogeneous (e.g., compared to the exponentially decaying waves), are inherited by the supermode. This allows one to maintain efficient and asymmetric coupling to a single quantum emitter located not only at a specific point but rather in a random point in the relatively large area.

III. ENGINEERING OF THE DISPERSION AND POLARIZATION IN COUPLED WAVEGUIDES

The group velocity of the coupled mode is determined by the weighted sum of the group velocities of the isolated modes; therefore, it can be equal to zero only if at least one of the modes is a backward wave, i.e., has a negative group velocity. This can be realized in two different ways. First, we consider the case when two quasidegenerate forward waves belong to a periodic waveguide, while the backward wave is supported by a homogeneous waveguide, as shown in the dispersion diagram in Fig. 2(a) with dashed lines. From what follows, we assign indices "1" and "2" to the modes of the periodic waveguide, and we assign the index "3" to the mode of the homogeneous waveguide. Although a homogeneous waveguide generally supports modes only with positive group velocity, in the considered system the mode effectively becomes a backward wave after the dispersion folding, which occurs due to its coupling with the periodic waveguide (see Supplemental Material [47], Sec. A). In an alternative design, the mode with a negative group velocity belongs to a periodic waveguide, while the mode of a homogeneous waveguide is a forward one [Fig. 2(b)].

Although these two designs have qualitative differences that are explained further, the physical insight into the determinants of the interaction between the waveguide modes can be gained from the analysis carried out within the same framework of the conventional coupled-mode theory (CMT) [48–50]. Once the characteristics of the modes of the isolated waveguides are known, e.g., from numerical simulations, one can find the eigenfrequencies ω of the coupled modes from the following matrix equation (see Supplemental Material [47], Sec. B for general formulation of the CMT and its application to both designs):

$$\mathbf{MA} = \omega\mathbf{A}, \tag{1}$$

where $\mathbf{M}$ is the 3×3 coupling matrix, and $\mathbf{A} = (a_1, a_2, a_3)^T$ is the vector of the amplitudes a of the three interacting modes. Generally, all variables in Eq. (1) depend on the Bloch wave number k, thus allowing one to obtain a dispersion $\omega(k)$ of the coupled modes and their field distributions. The elements of the coupling matrix $\mathbf{M}$ can be adjusted in a wide range of values by tuning the geometrical parameters of the considered structures. For instance, the diagonal elements are mostly determined by the dispersion of the modes of the isolated waveguides, and they can be tuned by changing the geometrical parameters of the isolated waveguides. The nondiagonal element M_{12} describes the coupling between the modes of the periodic waveguide and its value is mostly influenced by the type of the asymmetry (with respect to xz plane)

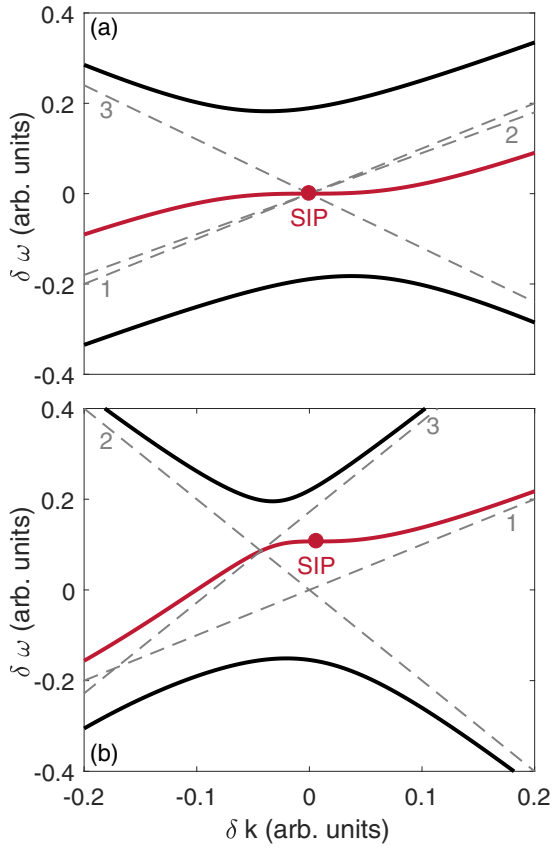

FIG. 2. Dispersion of the modes of coupled waveguides (solid curves) calculated within the framework of the CMT. Stationary inflection point is marked with a red circle. Dashed lines correspond to the modes of the isolated waveguides. Parameters of the system are as follows. (a) Group velocities $v_{g1} = 1$, $v_{g2} = 0.9$, and $v_{g3} = -1.2$; frequency detuning of the third mode $\Delta_3 = 0$; coupling constants $M_{12} = -0.1258$, $M_{13} = 0.1i$, and $M_{23} = 0.1$. The eigenvector at the SIP is $(1, i, 1.258)^T$. (b) Group velocities $v_{g1} = 1$, $v_{g2} = -2$, and $v_{g3} = 2$; frequency detuning of the third mode $\Delta_3 = 0.172$; coupling constants $M_{12} = -0.145i$, $M_{13} = 0.077$, and $M_{23} = 0$. The eigenvector at the SIP is $(1, 1.2i, -0.97)^T$.

introduced in the initially symmetric periodic waveguide. In turn, the elements M_{13} and M_{23} that describe the interaction between the modes of periodic and homogeneous waveguides are mostly determined by the distance between the waveguides. The relations between the geometrical parameters of the system and the elements of the matrix **M** are described in the Supplemental Material [47], Sec. C.

Using the formalism of the CMT one can analyze the requirements to the elements of the coupling matrix that allow one to achieve the desired characteristics of the waveguide, i.e., dispersion with a SIP and circular polarization of the local electric field in the periodic waveguide. To derive such requirements, we impose the following conditions on the eigenmode of Eq. (1) at the wave number k_0:

$$\left.\frac{d\omega}{dk}\right|_{k=k_0} = 0, \quad \left.\frac{d^2\omega}{dk^2}\right|_{k=k_0} = 0, \tag{2}$$

$$\mathbf{A}(k_0) = (1, i\alpha, \beta)^T, \tag{3}$$

where α and β are arbitrary real numbers (the phase of the third mode can be chosen at will). Equation (2) specifies the existence of the SIP, $\omega(k) \approx \omega(k_0) + \gamma(\delta k)^3$, at the point k_0, while the eigenvector (3) ensures the desired polarization of the field in the periodic waveguide. Note that we are interested in the circularly polarized electric field rather than the circularly polarized eigenvector **A** of the coupled mode; therefore, the coefficient α in a realistic design should be imaginary but its amplitude should not be necessarily equal to 1.

In Figs. 2(a) and 2(b) we show two dispersion diagrams of the coupled waveguides with the parameters that satisfy the conditions (2) and (3). In Fig. 2(a), the third mode has negative group velocity, while in Fig. 2(b) the second mode has negative group velocity. In the first case, we have found that the conditions (2) and (3) can be fulfilled when, first, all three modes intersect at the same point $k_0 = 0$ and, second, the elements M_{12} and M_{23} are real, while M_{13} is imaginary, resulting in the eigenvector with $\alpha = \mathrm{Im}(M_{13})/M_{23}$ and $\beta = -M_{12}/M_{23}$. In this case, the $\pm\pi/2$ phase difference between modes 1 and 2 is ensured by the zero phase of the coefficient M_{12}, while the magnitude of α is defined by the ratio $|M_{13}/M_{23}|$, which is of the order of 1 in realistic systems due to the quasidegeneracy of the first two modes. In the second case, Fig. 2(b), mode 2 has negative group velocity and therefore it typically interacts weakly with mode 3, and we assume that $M_{23} = 0$. In this case, first, we need to properly tune the frequency detuning of the third mode Δ and the amplitudes of the coupling constants M_{12} and M_{13}, and second, in contrast to the first design the M_{12} constant should be imaginary, as we demonstrate in the Supplemental Material [47], Sec. B.

Although, in these simple calculations we assumed that nondiagonal elements of the matrix **M** do not depend on k, and diagonal elements are linear functions of k, such simplification allowed us to identify the critical requirements to the waveguide design used in the following section.

IV. DESIGNS OF THE WAVEGUIDES BASED ON STRUCTURED SEMICONDUCTOR MEMBRANES

In order to demonstrate the feasibility of the proposed approach in the design of realistic optical structures we have developed two designs of the coupled waveguides based on the nanostructured GaAs membranes with the refractive index $n = 3.5$. The parameters of the structures were tuned to a wavelength around 950 nm corresponding to the emission wavelength of the InGaAs quantum dots. The schemes of the structures are shown in Figs. 3(a) and 3(d) with the geometrical parameters given in the caption. In Figs. 3(b) and 3(e) we show the dispersion properties of isolated and coupled waveguides with dashed gray and thick solid red curves, respectively. As it follows from the CMT, the distance between the waveguides d mainly affects the relative contribution of the mode of the homogeneous waveguide to the supermode, which in turn affects its group velocity. This can be observed in Figs. 3(c) and 3(f): by adjusting the distance d, it is formally possible to achieve an ideal SIP. We have chosen the optimal values of d so that the structure supports a single mode with the group velocity value around $c/200$ (where c is the speed of light) near the operational frequency marked with a black circle in Figs. 3(c) and 3(f).

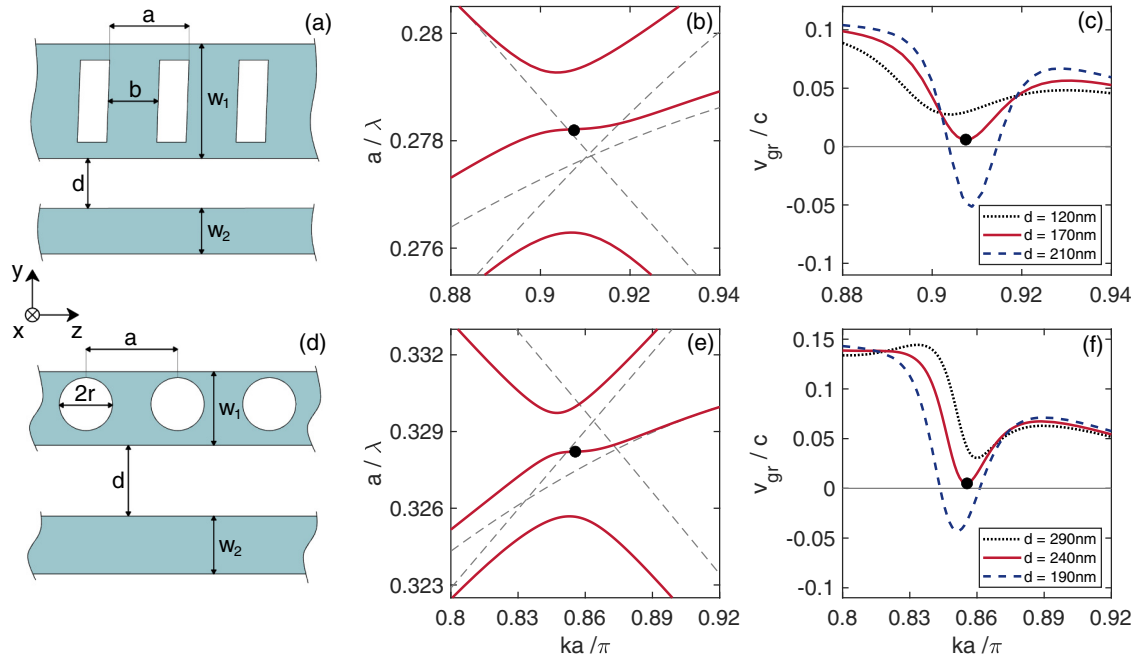

FIG. 3. (a), (d) Schemes of the guided structures under consideration (top view): (a) $a = 270$ nm, $b = 170$ nm, $w_1 = 390$ nm, $w_2 = 154$ nm, $d = 170$ nm, thickness of the membrane $h = 220$ nm, shift between the upper and lower vertices of the hole in the z direction is 10 nm; (b) $a = 310$ nm, $r = 90$ nm, $w_1 = 250$ nm, $w_2 = 197$ nm, $d = 240$ nm, $h = 245$ nm, shift of the holes in the y direction is $\delta y = 15$ nm. (b), (e) Dispersion of the modes of the isolated (gray dashed curves) and coupled (solid red curves) waveguides for the structures shown in panels (a) and (d), respectively. Black dots indicate the SIPs. (c), (f) Group velocity of the mode with a SIP as a function of the wave number for three values of the gap between the waveguides.

Besides the evanescent coupling between the waveguides, the modes of the periodic waveguide were also coupled with each other due to slight asymmetry introduced to the waveguide: in the first design the rectangular holes were modified by the slight shear deformation in the z direction, and in the second design the circular holes were shifted in the y direction by a small distance δy. By doing this the coupling constant M_{12} satisfied the previously derived conditions and the modes of the periodic waveguide were coupled with the $\pi/2$ phase difference, providing the local circular polarization of the electric field. In order to quantify the resulting polarization properties of the waveguide and the slow-light enhancement of a dipole emission at the same time, we have performed calculations of the coupling strength of a dipole QE to a waveguide mode γ_{WG} using Fermi's golden rule, i.e., assuming weak interaction. Within this framework, γ_{WG} normalized by the decay rate in the bulk material γ_0 is found using the following formula [22,51]:

$$\frac{\gamma^{\pm}_{WG}}{\gamma_0} = \frac{3\pi c^3 a |\mathbf{E}^{\pm}(\mathbf{r}_d)\cdot\mathbf{d}^*|^2}{2\omega_d^2\sqrt{\varepsilon}v_g}, \tag{4}$$

where c is speed of light, a is the waveguide period, ω_d is the dipole oscillation frequency, v_g is the eigenmode group velocity, ε is the permittivity of the waveguide material, $\mathbf{r}_d$ is the radius vector that defines the position of the dipole with unit vector $\mathbf{d}$, and $\mathbf{E}^{\pm}$ is the electric field distribution of the modes propagating in positive and negative z directions, respectively, normalized in such a way that $\int_{\text{unit cell}} \varepsilon|\mathbf{E}|^2 dV = 1$. We calculate this quantity for the fixed polarization of the dipole source $\mathbf{d} = (0, 1, i)/\sqrt{2}$ located in the plane $x = \pm 90$ nm and oscillating at the frequency that corresponds to the SIP. Note that since the fields of the modes propagating in opposite directions are related via complex conjugation, the change of the handedness of the dipole source results in the interchange between the decay rates γ^{+}_{WG} and γ^{-}_{WG}.

The results of calculations are presented in Fig. 4. One can observe that the coupling rate of the dipole source to the mode propagating in the positive z direction, γ^{+}_{WG}, normalized by the rate of emission in the bulk semiconductor γ_0 [Figs. 4(a) and 4(d)] reaches values up to 10 in both designs, and it is much stronger than the coupling to the mode propagating in the negative z direction, γ^{-}_{WG} [Figs. 4(b) and 4(e)], in most parts of the periodic waveguide cross section. The directivity of the emission D, calculated as $D = (\gamma^{+}_{WG} - \gamma^{-}_{WG})/(\gamma^{+}_{WG} + \gamma^{-}_{WG})$, reaches values close to 1 in most parts of the waveguide cross section. The asymmetry of the directivity distribution with respect to the $y = 0$ plane is caused by the interference of the even and odd modes supported by the periodic waveguide as well as by the asymmetric perturbation introduced in the unit cell.

In order to better illustrate the robustness of the coupling asymmetry to the position of the QE, we have introduced the figure of merit that characterizes the average directivity of emission of a randomly located point dipole source defined as $D_{av} = \langle\gamma^{+}_{WG} - \gamma^{-}_{WG}\rangle/\langle\gamma^{+}_{WG} + \gamma^{-}_{WG}\rangle$, where averaging is performed over the cross-sectional area of the periodic waveguide in the plane $x = 90$ nm. Figure 4(g) shows that for the chosen parameters D_{av} reaches at least $\approx$0.65 in both cases. Such a

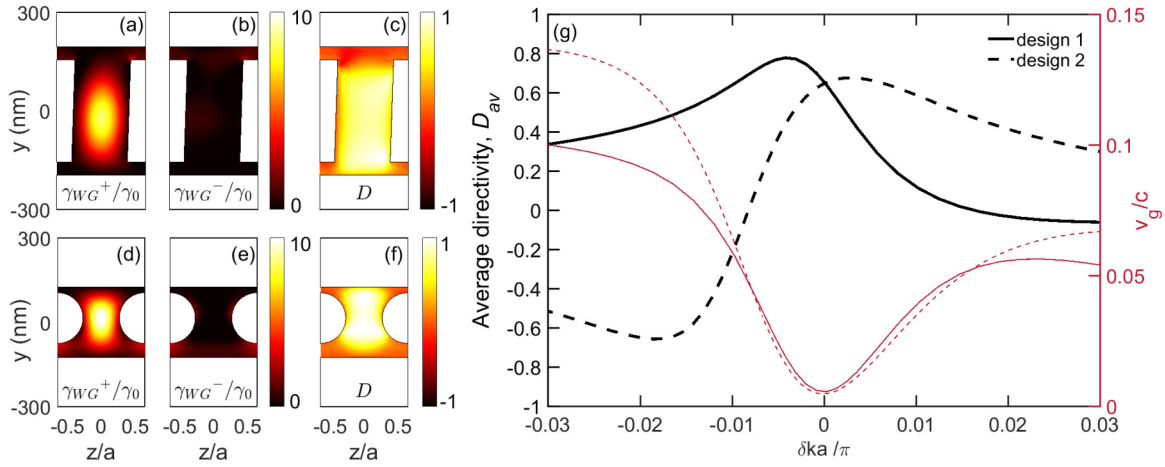

FIG. 4. (a), (b), (d), (e) Emission rate of the slow-light mode propagating in (a), (d) the positive z direction and (b), (e) the negative z direction as a function of the position of a CP dipole source in the cross section $x = 90$ nm of the periodic waveguide. (c), (f) Directivity of the emission. Panels (a)–(c) correspond to the first design, and panels (d)–(f) correspond to the second one. (g) Average directivity D_{av} (black curves, left axis) and normalized group velocity (red curves, right axis) as a function of the normalized wave number detuning. Zero detuning corresponds to the minimum group velocity. Solid curves correspond to the first design, and dashed curves correspond to the second one.

high value of the average asymmetry becomes possible due to the locked $\pi/2$ phase difference between two guided modes with orthogonal polarization of the electric field, achieved by proper engineering of the coupling between the waveguides. Note that a somewhat similar approach to achieve an efficient unidirectional coupling robust to the position of the source based on a photonic crystal cavity with two quasidegenerate modes was recently reported [52].

V. ESTIMATION OF THE β FACTOR

Although the main characteristics of the coupling between the dipole source and the waveguide can be well understood from the eigenmode simulations, these characteristics lack the information about the coupling strength of the dipole to all other modes of the surrounding environment. In order to estimate the β factor, which is the ratio of the decay rate to the given waveguide mode and the total decay rate $\beta = \gamma_{WG}/\gamma$, we have performed direct numerical simulations of the finite-size structure fed by a quasipoint dipolelike source. Since there is no qualitative difference in the characteristics of both designs, further we present the results only for the second design.

Calculation of the β factor to the infinite periodic waveguide is not a straightforward problem due to the necessity of applying the special boundary conditions that will absorb the propagating mode [53]. Such a problem is especially complicated when the considered guided mode has a slow group velocity [54]. In our simulations we have considered a finite-size waveguide with the adiabatic absorbers at the end of the waveguide fed by a circularly polarized dipole source with two possible polarizations $\mathbf{d}^{\pm} = (\mathbf{e}_y \pm i\mathbf{e}_z)/\sqrt{2}$ placed at the point with coordinates $\mathbf{r} = (90, -25, 0)$ nm, where maximum coupling asymmetry was expected. From the simulations we have extracted the power emitted into waveguide modes propagating in positive and negative z directions as well as the power radiated into free space and other modes of the system. In order to check the validity of the results we have performed several simulations varying the size of the waveguide and the absorbing part, making sure that the corresponding variation of the power coupled to the waveguide and the β factor becomes insignificant. Additionally, we have calculated the power emitted by the same source in the bulk semiconductor γ_0 and compared the results of the ratio γ_{WG}/γ_0 obtained in the simulations with the source and the eigenmodes simulations.

The results of calculations of the emission enhancement factor into the waveguide $\gamma_{WG}^{\pm}/\gamma_0$ are presented in Fig. 5(a). The peak value of $\gamma_{WG}^{+}/\gamma_0 \approx 8$ is in a good agreement with

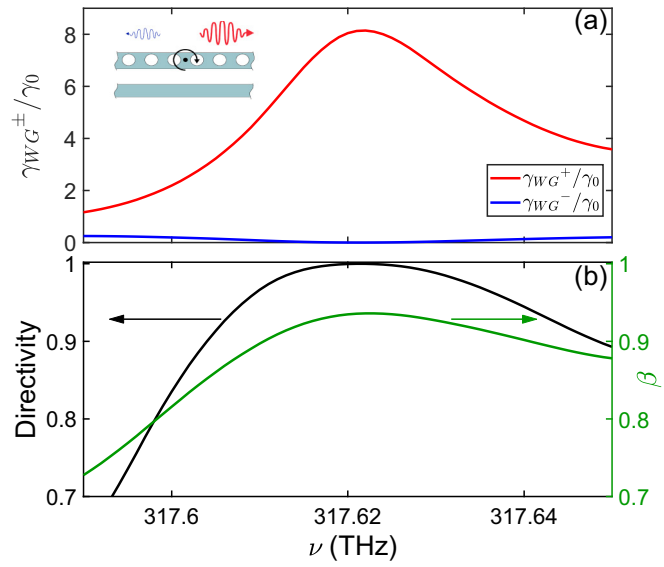

FIG. 5. (a) Rate of emission of a circularly polarized dipole source into the slow-light mode propagating in the positive z direction γ_{WG}^{+} (solid red) and the negative z direction γ_{WG}^{-} (solid blue) normalized by the emission rate in a bulk semiconductor γ_0 as a function of frequency. (b) Directivity (black curve, left axis) and β factor (green curve, right axis) as a function of frequency.

$\gamma^{+}_{WG}/\gamma_0 \approx 8.5$ obtained from the eigenmode simulations for the given position and polarization of the source [Fig. 4(c)], which confirms that the simulations of the system with the dipole source provide reliable characteristics of the structure. The substantial difference between γ^{+}_{WG} and γ^{-}_{WG} rates leads to the almost perfect directivity near the frequency corresponding to the SIP [see the black curve in Fig. 5(b)]. The β factor at the same time reaches values up to 94%. Note that theoretically it is possible to increase the coupling to the waveguide modes, and consequently the β factor, in an unlimited way by fine tuning of the system parameters. The current values were obtained for experimentally achievable group indices as large as 200.

VI. SUMMARY

To summarize we have demonstrated a possibility of enhancement of the chiral light-matter interaction in the periodic dielectric waveguides through simultaneous engineering of the stationary inflection point in the dispersion and tailoring local polarization of the electric field by exploiting a multimode regime of the waveguides. Highly efficient and directive emission of the circularly polarized dipole sources into the desired guided mode was demonstrated in numerical simulations. Along with the robustness of the system to the position of the source, this makes the proposed design promising for the further development of the planar integrated spin-photon interfaces enabled by the spin-orbit interactions of light.

ACKNOWLEDGMENTS

This work was supported by the Russian Science Foundation, Grant No. 19-72-10129. The calculations of the directivity were supported by a grant from the President of the Russian Federation, Grant No. MK-4418.2021.1.2.

[1] P. Lodahl, S. Mahmoodian, S. Stobbe, A. Rauschenbeutel, P. Schneeweiss, J. Volz, H. Pichler, and P. Zoller, Chiral quantum optics, Nature (London) **541**, 473 (2017).

[2] C. Junge, D. O'Shea, J. Volz, and A. Rauschenbeutel, Strong Coupling between Single Atoms and Nontransversal Photons, Phys. Rev. Lett. **110**, 213604 (2013).

[3] C. Sayrin, C. Junge, R. Mitsch, B. Albrecht, D. O'Shea, P. Schneeweiss, J. Volz, and A. Rauschenbeutel, Nanophotonic Optical Isolator Controlled by the Internal State of Cold Atoms, Phys. Rev. X **5**, 041036 (2015).

[4] M. Scheucher, A. Hilico, E. Will, J. Volz, and A. Rauschenbeutel, Quantum optical circulator controlled by a single chirally coupled atom, Science **354**, 1577 (2016).

[5] P. Lodahl, Quantum-dot based photonic quantum networks, Quantum Sci. Technol. **3**, 013001 (2017).

[6] P. Chen, T. W. Lo, Y. Fan, S. Wang, H. Huang, and D. Lei, Chiral coupling of valley excitons and light through photonic spin–orbit interactions, Adv. Opt. Mater. **8**, 1901233 (2020).

[7] A. B. Young, A. C. T. Thijssen, D. M. Beggs, P. Androvitsaneas, L. Kuipers, J. G. Rarity, S. Hughes, and R. Oulton, Polarization Engineering in Photonic Crystal Waveguides for Spin-Photon Entanglers, Phys. Rev. Lett. **115**, 153901 (2015).

[8] I. Söllner, S. Mahmoodian, S. L. Hansen, L. Midolo, A. Javadi, G. Kiršanskė, T. Pregnolato, H. El-Ella, E. H. Lee, J. D. Song, S. Stobbe, and P. Lodahl, Deterministic photon–emitter coupling in chiral photonic circuits, Nat. Nanotechnol. **10**, 775 (2015).

[9] I. J. Luxmoore, N. A. Wasley, A. J. Ramsay, A. C. T. Thijssen, R. Oulton, M. Hugues, A. M. Fox, and M. S. Skolnick, Optical control of the emission direction of a quantum dot, Appl. Phys. Lett. **103**, 241102 (2013).

[10] R. J. Coles, D. M. Price, J. E. Dixon, B. Royall, E. Clarke, P. Kok, M. S. Skolnick, A. M. Fox, and M. N. Makhonin, Chirality of nanophotonic waveguide with embedded quantum emitter for unidirectional spin transfer, Nat. Commun. **7**, 11183 (2016).

[11] D. L. Hurst, D. M. Price, C. Bentham, M. N. Makhonin, B. Royall, E. Clarke, P. Kok, L. R. Wilson, M. S. Skolnick, and A. M. Fox, Nonreciprocal transmission and reflection of a chirally coupled quantum dot, Nano Lett. **18**, 5475 (2018).

[12] A. Javadi, D. Ding, M. H. Appel, S. Mahmoodian, M. C. Löbl, I. Söllner, R. Schott, C. Papon, T. Pregnolato, S. Stobbe, L. Midolo, T. Schröder, A. D. Wieck, A. Ludwig, R. J. Warburton, and P. Lodahl, Spin-photon interface and spin-controlled photon switching in a nanobeam waveguide, Nat. Nanotechnol. **13**, 398 (2018).

[13] S. Xiao, S. Wu, X. Xie, J. Yang, W. Wei, S. Shi, F. Song, J. Dang, S. Sun, L. Yang, Y. Wang, S. Yan, Z. Zuo, T. Wang, J. Zhang, K. Jin, and X. Xu, Chiral photonic circuits for deterministic spin transfer, Laser Photonics Rev. **15**, 2100009 (2021).

[14] I. Shomroni, S. Rosenblum, Y. Lovsky, O. Bechler, G. Guendelman, and B. Dayan, All-optical routing of single photons by a one-atom switch controlled by a single photon, Science **345**, 903 (2014).

[15] D. Martin-Cano, H. R. Haakh, and N. Rotenberg, Chiral emission into nanophotonic resonators, ACS Photonics **6**, 961 (2019).

[16] S. Barik, A. Karasahin, S. Mittal, E. Waks, and M. Hafezi, Chiral quantum optics using a topological resonator, Phys. Rev. B **101**, 205303 (2020).

[17] M. Jalali Mehrabad, A. P. Foster, R. Dost, E. Clarke, P. K. Patil, I. Farrer, J. Heffernan, M. S. Skolnick, and L. R. Wilson, A semiconductor topological photonic ring resonator, Appl. Phys. Lett. **116**, 061102 (2020).

[18] M. J. Mehrabad, A. P. Foster, R. Dost, E. Clarke, P. K. Patil, A. M. Fox, M. S. Skolnick, and L. R. Wilson, Chiral topological photonics with an embedded quantum emitter, Optica **7**, 1690 (2020).

[19] W.-S. Ruan, X.-T. He, F.-L. Zhao, and J.-W. Dong, Analysis of unidirectional coupling in topological valley photonic crystal waveguides, J. Lightwave Technol. **39**, 889 (2021).

[20] P. Lodahl, S. Mahmoodian, and S. Stobbe, Interfacing single photons and single quantum dots with photonic nanostructures, Rev. Mod. Phys. **87**, 347 (2015).

[21] C. P. Dietrich, A. Fiore, M. G. Thompson, M. Kamp, and S. Höfling, Gaas integrated quantum photonics: Towards compact and multi-functional quantum photonic integrated circuits, Laser Photonics Rev. **10**, 870 (2016).

[22] B. Le Feber, N. Rotenberg, and L. Kuipers, Nanophotonic control of circular dipole emission, Nat. Commun. **6**, 6695 (2015).

[23] T. Pregnolato, X.-L. Chu, T. Schröder, R. Schott, A. D. Wieck, A. Ludwig, P. Lodahl, and N. Rotenberg, Deterministic positioning of nanophotonic waveguides around single self-assembled quantum dots, APL Photonics **5**, 086101 (2020).

[24] A. Krasnok, S. Makarov, M. Petrov, R. Savelev, P. Belov, and Y. Kivshar, Towards all-dielectric metamaterials and nanophotonics, Proc. SPIE **9502**, 950203 (2015).

[25] A. I. Kuznetsov, A. E. Miroshnichenko, M. L. Brongersma, Y. S. Kivshar, and B. Luk'yanchuk, Optically resonant dielectric nanostructures, Science **354**, aag2472 (2016).

[26] R. Regmi, J. Berthelot, P. M. Winkler, M. Mivelle, J. Proust, F. Bedu, I. Ozerov, T. Begou, J. Lumeau, H. Rigneault, M. F. García-Parajó, S. Bidault, J. Wenger, and N. Bonod, All-dielectric silicon nanogap antennas to enhance the fluorescence of single molecules, Nano Lett. **16**, 5143 (2016).

[27] D. Bouchet, M. Mivelle, J. Proust, B. Gallas, I. Ozerov, M. F. Garcia-Parajo, A. Gulinatti, I. Rech, Y. De Wilde, N. Bonod, V. Krachmalnicoff, and S. Bidault, Enhancement and Inhibition of Spontaneous Photon Emission by Resonant Silicon Nanoantennas, Phys. Rev. Appl. **6**, 064016 (2016).

[28] V. Rutckaia, F. Heyroth, A. Novikov, M. Shaleev, M. Petrov, and J. Schilling, Quantum dot emission driven by Mie resonances in silicon nanostructures, Nano Lett. **17**, 6886 (2017).

[29] A. S. Zalogina, R. S. Savelev, E. V. Ushakova, G. P. Zograf, F. E. Komissarenko, V. A. Milichko, S. V. Makarov, D. A. Zuev, and I. V. Shadrivov, Purcell effect in active diamond nanoantennas, Nanoscale **10**, 8721 (2018).

[30] M. Sanz-Paz, C. Ernandes, J. U. Esparza, G. W. Burr, N. F. Van Hulst, A. Maitre, L. Aigouy, T. Gacoin, N. Bonod, M. F. Garcia-Parajo, S. Bidault, and M. Mivelle, Enhancing magnetic light emission with all-dielectric optical nanoantennas, Nano Lett. **18**, 3481 (2018).

[31] A. Krasnok, S. Glybovski, M. Petrov, S. Makarov, R. Savelev, P. Belov, C. Simovski, and Y. Kivshar, Demonstration of the enhanced Purcell factor in all-dielectric structures, Appl. Phys. Lett. **108**, 211105 (2016).

[32] A. Krasnok, S. Li, S. Lepeshov, R. Savelev, D. G. Baranov, and A. Alú, All-Optical Switching and Unidirectional Plasmon Launching with Nonlinear Dielectric Nanoantennas, Phys. Rev. Appl. **9**, 014015 (2018).

[33] T. X. Hoang, S. T. Ha, Z. Pan, W. K. Phua, R. Paniagua-Dominguez, C. E. Png, H.-S. Chu, and A. I. Kuznetsov, Collective Mie resonances for directional on-chip nanolasers, Nano Lett. **20**, 5655 (2020).

[34] V. Rutckaia, F. Heyroth, G. Schmidt, A. Novikov, M. Shaleev, R. S. Savelev, J. Schilling, and M. Petrov, Coupling of germanium quantum dots with collective sub-radiant modes of silicon nanopillar arrays, ACS Photonics **8**, 209 (2020).

[35] I. Staude, T. Pertsch, and Y. S. Kivshar, All-dielectric resonant meta-optics lightens up, ACS Photonics **6**, 802 (2019).

[36] A. Vaskin, R. Kolkowski, A. F. Koenderink, and I. Staude, Light-emitting metasurfaces, Nanophotonics **8**, 1151 (2019).

[37] R. Halir, P. J. Bock, P. Cheben, A. Ortega-Moñux, C. Alonso-Ramos, J. H. Schmid, J. Lapointe, D.-X. Xu, J. G. Wangüemert-Pérez, I. Molina-Fernández, and S. Janz, Waveguide sub-wavelength structures: A review of principles and applications, Laser Photonics Rev. **9**, 25 (2015).

[38] R. M. Bakker, Y. F. Yu, R. Paniagua-Dominguez, B. Luk'yanchuk, and A. I. Kuznetsov, Resonant light guiding along a chain of silicon nanoparticles, Nano Lett. **17**, 3458 (2017).

[39] P. Cheben, R. Halir, J. Schmid, H. Atwater, and D. Smith, Subwavelength integrated photonics, Nature (London) **560**, 565 (2018).

[40] L. Ding, D. Morits, R. Bakker, S. Li, D. Eschimese, S. Zhu, Y. F. Yu, R. Paniagua-Dominguez, and A. I. Kuznetsov, All-optical modulation in chains of silicon nanoantennas, ACS Photonics **7**, 1001 (2020).

[41] O. Y. Yermakov, A. A. Bogdanov, and A. V. Lavrinenko, Broadband polarization degeneracy of guided waves in sub-wavelength structured ZnO pattern, IEEE J. Sel. Top. Quantum Electron. **25**, 1 (2019).

[42] R. S. Savelev, D. F. Kornovan, V. V. Yaroshenko, and M. I. Petrov, Analogue of the Kerker effect for localized modes of discrete high-index dielectric nanowaveguides, J. Appl. Phys. **125**, 123104 (2019).

[43] R. S. Savelev and M. A. Gorlach, Topological states in arrays of optical waveguides engineered via mode interference, Phys. Rev. B **102**, 161112(R) (2020).

[44] N. Gutman, W. H. Dupree, Y. Sun, A. A. Sukhorukov, and C. M. de Sterke, Frozen and broadband slow light in coupled periodic nanowire waveguides, Opt. Express **20**, 3519 (2012).

[45] M. Y. Nada, M. A. K. Othman, and F. Capolino, Theory of coupled resonator optical waveguides exhibiting high-order exceptional points of degeneracy, Phys. Rev. B **96**, 184304 (2017).

[46] M. Y. Nada, T. Mealy, and F. Capolino, Frozen mode in three-way periodic microstrip coupled waveguide, IEEE Microwave Wireless Compon. Lett. **31**, 229 (2021).

[47] See Supplemental Material at http://link.aps.org/supplemental/10.1103/PhysRevB.104.245408 for the details on the optical properties of the isolated waveguides, the formulation of the coupled-mode theory, and the relation between the geometrical parameters of the structure and the coupled-mode theory.

[48] A. Yariv and P. Yeh, *Optical Waves in Crystals: Propagation and Control of Laser Radiation* (Wiley & Sons, New York, 2003).

[49] A. A. Sukhorukov, A. V. Lavrinenko, D. N. Chigrin, D. E. Pelinovsky, and Y. S. Kivshar, Slow-light dispersion in coupled periodic waveguides, J. Opt. Soc. Am. B **25**, C65 (2008).

[50] S. G. Johnson, M. Ibanescu, M. A. Skorobogatiy, O. Weisberg, J. D. Joannopoulos, and Y. Fink, Perturbation theory for Maxwell's equations with shifting material boundaries, Phys. Rev. E **65**, 066611 (2002).

[51] V. S. C. Manga Rao and S. Hughes, Single quantum-dot Purcell factor and β factor in a photonic crystal waveguide, Phys. Rev. B **75**, 205437 (2007).

[52] D. Hallett, A. P. Foster, D. M. Whittaker, M. S. Skolnick, and L. R. Wilson, arXiv:2108.01462.

[53] A. Javadi, S. Mahmoodian, I. Söllner, and P. Lodahl, Numerical modeling of the coupling efficiency of single quantum emitters in photonic-crystal waveguides, J. Opt. Soc. Am. B **35**, 514 (2018).

[54] A. F. Oskooi, L. Zhang, Y. Avniel, and S. G. Johnson, The failure of perfectly matched layers, and towards their redemption by adiabatic absorbers, Opt. Express **16**, 11376 (2008).